

Electron-Photon Chern Number in Cavity-Embedded 2D Moiré MaterialsDanh-Phuong Nguyen¹, Geva Arwas,¹ Zuzhang Lin^{2,3}, Wang Yao,^{2,3} and Cristiano Ciuti¹¹Université Paris Cité, CNRS, Matériaux et Phénomènes Quantiques, 75013 Paris, France²Department of Physics, The University of Hong Kong, Hong Kong, China³HKU-UCAS Joint Institute of Theoretical and Computational Physics at Hong Kong, China (Received 28 March 2023; revised 11 September 2023; accepted 25 September 2023; published 25 October 2023)

We explore theoretically how the topological properties of 2D materials can be manipulated by cavity quantum electromagnetic fields for both resonant and off-resonant electron-photon coupling, with a focus on van der Waals moiré superlattices. We investigate an electron-photon topological Chern number for the cavity-dressed energy minibands that is well defined for any degree of hybridization and entanglement of the electron and photon states. While an off-resonant cavity mode can renormalize electronic topological phases that exist without cavity coupling, we show that when the cavity mode is resonant to electronic miniband transitions, new and higher electron-photon Chern numbers can emerge.

DOI: [10.1103/PhysRevLett.131.176602](https://doi.org/10.1103/PhysRevLett.131.176602)

Introduction.—In recent years van der Waals heterostructures combining atomic-thin layers of 2D materials such as graphene or transition metal dichalcogenides (TMD) have attracted a great deal of interest [1–6]. Indeed, these systems present rich and controllable physical properties already at the single-particle level due to multiple quantum degrees of freedom, namely the electron spin, the valley, and layer pseudospins. This class of 2D materials exhibits a wide variety of interesting electronic properties including semi-metallic, semiconducting, superconducting, and magnetic phases. One prominent example is magic angle twisted bilayer graphene, exhibiting quasiflat electronic bands [7] and remarkable superconducting properties [8]. Another notable class of moiré heterostructures is based on TMD materials, which, thanks to their semiconductor properties, have particularly interesting optical properties [9–11].

A growing interest is emerging for the manipulation of materials with cavity vacuum fields [12–15]. In particular, metallic split-ring terahertz electromagnetic resonators are remarkable for their deeply subwavelength photon mode confinement [16–18] with mode volumes that can be as small as $10^{-10}\lambda_0^3$, λ_0 being the free-space electromagnetic wavelength corresponding to the resonator frequency. Studies on GaAs 2D electron gases have shown that electronic transport in mesoscopic quantum Hall bars can be greatly modified by the coupling to electromagnetic resonators even without illumination [19], as a result of cavity-mediated electron hopping [20,21], which results in a breakdown of the Hall resistance quantization associated to the topological properties of the electronic Landau states.

Recent theoretical works have investigated how to exploit cavity QED to control topological properties of systems, such as 1D tight-binding chains described by the Su-Schrieffer-Heeger model [22]. Concerning 2D systems, a recent work has studied 2D bulk materials [23,24] where

the standard electron Chern number is computed by considering an effective electronic Hamiltonian obtained by adiabatic elimination of the photon degrees of freedom. A Letter exploring single-sheet graphene ribbons [25] has studied electron Chern numbers computed once the cavity field is approximated in a classical coherent state. Another investigation has explored a generic single-electron problem in the ultrastrong light-matter coupling regime [26] and focused on the topological control in the configuration where the cavity photon mode frequency is much larger than the relevant electronic transition frequencies. A key point that has not been addressed is the behavior of genuine electron-photon topological invariants that are associated to the interacting quantum electron-photon system when the photon mode is resonant to electronic transitions. In the past, this has been done only for classical exciton-polariton normal modes where a bosonic exciton field is strongly coupled to a cavity photon field [27,28] (the bare cavity photon and exciton bands are topologically trivial, but the hybrid light-matter polariton bands are not). However, for a fermionic particle coupled to a quantized cavity field, to the best of our knowledge, the study of electron-photon topological invariants for the resonant light-matter coupling has been overlooked.

In this Letter, we explore the properties of electron-photon Chern numbers, focusing on cavity-embedded 2D moiré materials. We investigate different regimes of coupling (off-resonant versus resonant cavity mode), for different cavity geometries (mode with in-plane or out-of-plane polarization) and explore the topological transitions characterized by such an electron-photon Chern number with realistic values for state-of-the-art split-ring resonators and TMD materials. We show that in the case of resonant electron-photon coupling, new topological phases and high Chern numbers can emerge.

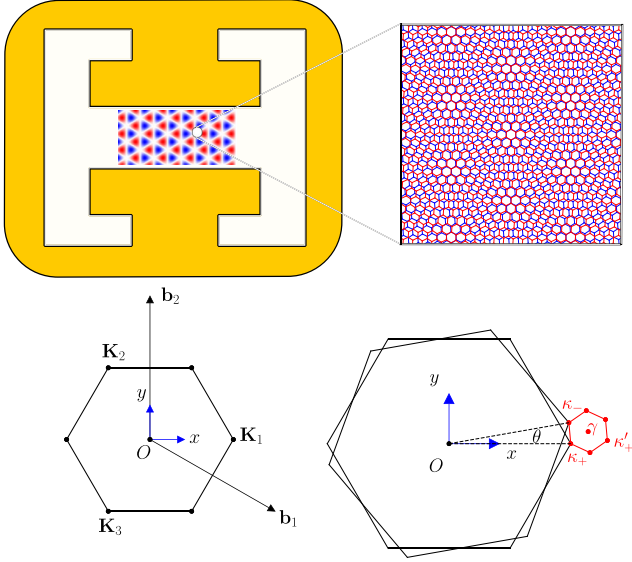


FIG. 1. Top: sketch of a twisted bilayer system with its moiré pattern inside the gap region of a split-ring resonator. Bottom: on the left, the first Brillouin zone with Dirac points of the bottom layer and corresponding wave vectors; on the right, the Brillouin zones of both the bottom and rotated top layer together with the moiré mini Brillouin zone (shown in red) for the corresponding moiré superlattice.

Cavity QED Hamiltonian.—Let us consider a bilayer moiré system consisting of two twisted TMD layers embedded in a single-mode resonator (see the sketch in Fig. 1). Each of them is a honeycomb lattice defined by two primitive translation vectors $\mathbf{a}_1 = a_0\sqrt{3}/2(1, \sqrt{3}, 0)$ and $\mathbf{a}_2 = a_0\sqrt{3}/2(-1, \sqrt{3}, 0)$, where a_0 is the monolayer TMD lattice constant. We consider in-plane parallel stacking (R stacking) with the layer on top rotated by a small angle θ in order to create a long wavelength moiré pattern. The distance between two layers is d . The moiré unit cell is defined by $\mathbf{L}_{i=1,2} = [\mathbb{1} - R(\theta)^{-1}]^{-1}\mathbf{a}_i$, where $\mathbb{1}$ and $R(\theta)$ are respectively the identity and the rotation matrix corresponding to the rotation angle θ about the z axis. We denote the moiré lattice constant $|\mathbf{L}_i|$ as a_M , where for small angles $a_M \simeq a_0/\theta$. In the following, for numerical applications we will use parameters of the MoTe₂ system [29]. For the photonic part, thanks to the approximately flat mode inside the capacitive gap of complementary split-ring resonators [19], we will consider a single-mode cavity with a spatially homogeneous field described by the vector potential $\hat{\mathbf{A}} = A_0\mathbf{u}(\hat{a} + \hat{a}^\dagger)$ with \hat{a}^\dagger

(\hat{a}) the photonic creation (annihilation) operator. The vacuum field amplitude is $A_0 = \sqrt{\hbar/(2\omega_c\epsilon_0V_{mode})}$ with ω_c the mode frequency, $V_{mode} = \eta\lambda_c^3$ the effective mode volume related to the compression factor η , and λ_c the wavelength in free space that corresponds to ω_c . The orientation of the cavity mode polarization is described by the unit vector $\mathbf{u} = (u_x, u_y, u_z)$.

Our treatment is based on the four-band continuum model for small angle twisted bilayer TMD [29,30]. The cavity QED Hamiltonian can be written as

$$\hat{H} = \hbar\omega_c\hat{a}^\dagger\hat{a} + \begin{pmatrix} \hat{H}_t & 0 \\ 0 & \hat{H}_b \end{pmatrix} + \begin{pmatrix} \hat{V}_t & \hat{U} \\ \hat{U}^\dagger & \hat{V}_b \end{pmatrix}, \quad (1)$$

where the 2×2 operator matrix \hat{H}_t (\hat{H}_b) corresponds to the conduction and valence bands of the top (bottom) layer. The moiré potentials are given by the last term. The light-matter coupling is introduced via Peierls factors [31] in the intralayer (\hat{H}_t , \hat{H}_b) and interlayer (\hat{U}) hopping terms. We quantify the interaction strength by the dimensionless constant $g = eA_0a_0/\hbar$. For $g \ll 1$ and in the low-energy sector, each diagonal block matrix $\nu = t, b$ and interlayer coupling \hat{U} can be approximated as follows:

$$\begin{aligned} \hat{H}_\nu &= \Delta\sigma_z + v_F\sigma_{xy} \left[\hat{\mathbf{p}} - \hbar\mathbf{K}_\nu + e\mathbf{A}^{(xy)}(\hat{a} + \hat{a}^\dagger) \right], \\ \hat{U} &= e^{-i\frac{eA^{(z)}d}{\hbar}(\hat{a} + \hat{a}^\dagger)} \hat{U}_0, \end{aligned} \quad (2)$$

with $\mathbf{K}_t = \boldsymbol{\kappa}_-$, $\mathbf{K}_b = \boldsymbol{\kappa}_+$ shown in Fig. 1, $\sigma_{xy} = (\sigma_x, \sigma_y, 0)$ a vector of Pauli matrices, $\mathbf{A}^{(xy)}$ is the in-plane projection of $A_0\mathbf{u}$, and $A^{(z)}$ is its z component. Note that the interlayer distance d is much larger than the in-plane lattice constant a_0 . Hence, the argument of the Peierls exponential for the U term is much larger than its t counterpart (in-plane coupling). We will consider a regime of realistic parameters, where it turns out that the exponential of the t term can be linearized, while the out-of-plane Peierls term must be kept in exponential form. The moiré potentials \hat{V}_ν and \hat{U}_0 are the same as the ones in [29,30]. Because of the large energy gap between the conduction and valence band in the TMD material, we can restrict our description to the latter, for which nontrivial topological properties were studied [29,32] in the absence of a cavity field. Finally, we represent the Hamiltonian in the hole picture. The corresponding Hamiltonian reads

$$\hat{\mathcal{H}} = \hbar\omega_c\hat{a}^\dagger\hat{a} + \frac{1}{2m^*} \begin{pmatrix} (\hat{\mathbf{p}} + \hbar\boldsymbol{\kappa}_- - e\mathbf{A}^{(xy)}(\hat{a} + \hat{a}^\dagger))^2 & 0 \\ 0 & (\hat{\mathbf{p}} + \hbar\boldsymbol{\kappa}_+ - e\mathbf{A}^{(xy)}(\hat{a} + \hat{a}^\dagger))^2 \end{pmatrix} - \begin{pmatrix} \hat{V}_t^v & \hat{U}_0^{v\dagger} \\ \hat{U}_0^v & \hat{V}_b^v \end{pmatrix} - i\frac{\omega_c e A^{(z)} d}{2} (\hat{a} - \hat{a}^\dagger) \tau_z \quad (3)$$

where $m^* = \Delta/v_F^2$ is the effective mass of the valence band, and τ_z is the z axis Pauli matrix with respect to the layer pseudospin. We have considered minimal coupling in the Coulomb gauge for the in-plane motion, while the dipole gauge resulting from a Power-Zienau-Woolley (PZW) transformation is used for the out-of-plane part. The expression for the moiré potentials $\hat{V}_t^v, \hat{V}_b^v, \hat{U}_0^v$ is the same as in [29,30] and is reported in the Supplemental Material [31]. To account for the interlayer bias V_z (that breaks the symmetry between κ_+ and κ_- [29]), the term $-V_z/2 \times \tau_z$ has to be added to the Hamiltonian in Eq. (3). As the moiré potential is periodic with respect to $\mathbf{L}_{i=1,2}$ translations, the electronic part can be block-diagonalized in momentum space (Bloch theorem). Each block \mathbf{k} belongs to the moiré mini Brillouin zone (mBZ) shown in Fig. 1, spanned by moiré reciprocal vectors \mathbf{G}_1 and \mathbf{G}_2 satisfying $\mathbf{G}_i \cdot \mathbf{L}_j = 2\pi\delta_{ij}$.

Definition of the electron-photon Chern number.—Let us consider a single fermion interacting with a cavity quantized field. This is equivalent to injecting a fermion into empty minibands. If the fermion wave vector \mathbf{k} is a good quantum number, then we can diagonalize the Hamiltonian $\hat{\mathcal{H}}_{\mathbf{k}} = e^{-i\mathbf{k}\cdot\hat{\mathbf{r}}}\hat{\mathcal{H}}e^{i\mathbf{k}\cdot\hat{\mathbf{r}}}$ and obtain electron-photon eigenstates of the form $|\Psi_{n\mathbf{k}}^{(e-p)}\rangle$ with corresponding electron-photon energy bands $\mathcal{E}_{n\mathbf{k}}^{(e-p)}$. Given the form of the system eigenstates, we can introduce the following electron-photon Chern number:

$$C_n^{(e-p)} = \int \frac{d^2k}{2\pi} i \sum_{\mu,\nu} \epsilon_{\mu\nu} \langle \partial_{k_\mu} \Psi_{n\mathbf{k}}^{(e-p)} | \partial_{k_\nu} \Psi_{n\mathbf{k}}^{(e-p)} \rangle, \quad (4)$$

where $\epsilon_{\mu\nu}$ is the two-dimensional Levi-Civita tensor. Importantly, the electron-photon Chern number in Eq. (4) is well defined for any arbitrary hybridization between the single electron and the cavity quantum field. If we work in the hole picture, the particle-hole transformation results in a simple change of sign of such Chern number. Numerically the Chern number in Eq. (4) has been calculated by numerical diagonalization of the Hamiltonian (3) and using the technique reported in Ref. [33].

Results and discussions.—In what follows, we use the electron-photon Chern number to investigate topological properties of cavity-embedded moiré systems, focusing on twisted MoTe₂ bilayers. We first consider the scenario of high photon frequency, where the photon is off-resonant with respect to the relevant miniband electronic transitions. In Fig. 2, we report the electron-photon topological Chern numbers associated with the first three moiré minibands of the twisted bilayer TMD system. Here, we consider a cavity mode with in-plane polarization $\mathbf{u} = (1, 0, 0)$. For $g = 0$ (no cavity coupling), the system is known to exhibit a topological transition as a function of the twisting angle θ (top panel) and as a function of the interlayer bias V_z (bottom panel). In the top panel we consider the case with

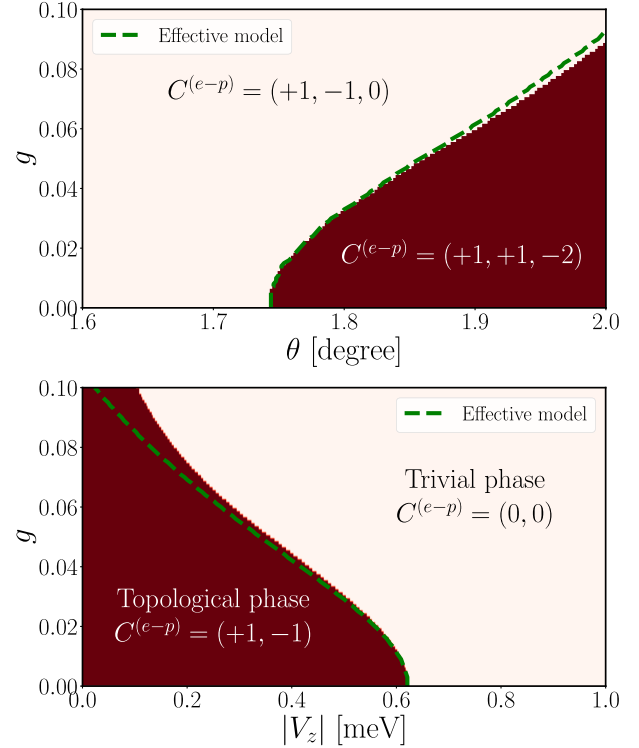


FIG. 2. Electron-photon Chern numbers of the first three (top) and two (bottom) moiré minibands of the twisted TMD bilayer system (MoTe₂ parameters). The dashed lines depict the phase boundary predicted by an effective electronic Hamiltonian obtained by adiabatically eliminating the photonic degrees of freedom [21] and calculating the electron Chern number. Top: Chern numbers versus the twisting angle θ and the dimensionless cavity coupling g (see definition in the text), with no interlayer bias ($V_z = 0$). Bottom: Chern numbers versus V_z and the dimensionless cavity coupling g for a fixed angle $\theta = 1.2^\circ$. Parameters: cavity photon energy $\hbar\omega_c = 20$ meV (top) and 6 meV (bottom), cavity mode polarization vector $\mathbf{u} = (1, 0, 0)$.

no bias ($V_z = 0$) for which a topological transition occurs by increasing the twisting angle θ above a critical value ($\approx 1.75^\circ$ at zero g), with Chern numbers changing from $(+1, -1, 0)$ to $(+1, +1, -2)$. The bottom panel corresponds to a situation with a fixed angle $\theta = 1.2^\circ$ for which a transition from topologically nontrivial Chern numbers $(+1, -1, 0)$ to the trivial $(0, 0, 0)$ is achieved when V_z is increased above a critical value (≈ 0.63 meV at zero g). In both situations considered in Fig. 2, a finite cavity coupling modifies the transition boundary significantly for a range of dimensionless coupling g , which is accessible with deeply subwavelength resonators. The energy-momentum dispersions with and without the cavity are compared for $V_z = 0.5$ meV in Fig. 3 for a ribbon geometry (periodic boundary conditions along the long direction). The left panel shows the presence of topological edge states that cross in energy for $g = 0$, while the right panel shows the opening of an edge gap in the presence of a cavity with $g = 0.05$. In other words, Fig. 3 shows the consequence of

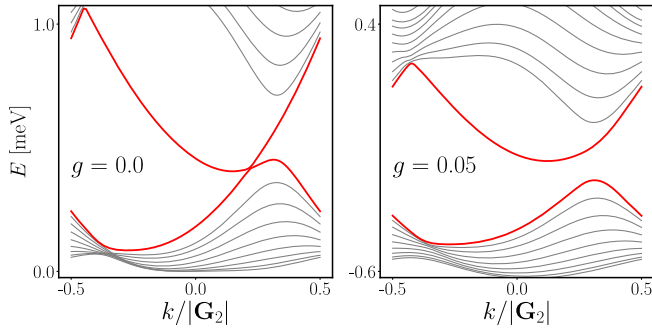


FIG. 3. Electron-photon energy-momentum dispersions $\mathcal{E}_{nk}^{(e-p)}$ for $g = 0.0$ (left) and 0.05 (right) for a ribbon geometry (periodic boundary conditions along the long direction). Parameters: cavity photon energy $\hbar\omega_c = 6$ meV, $V_z = 0.5$ meV, $\theta = 1.2^\circ$, ribbon width $D_1/a_M = 10$, and cavity mode polarization vector $\mathbf{u} = (1, 0, 0)$. Here, the photonic component of the electron-photon eigenstates is small (see text).

the topological transition with increasing cavity coupling g depicted in the diagram of the bottom panel in Fig. 2.

Note that by tracing out the photonic degrees of freedom, we can obtain an electronic reduced density matrix, namely $\hat{\rho}_{nk} = \text{Tr}_{\text{phot}}(|\Psi_{nk}^{(e-p)}\rangle\langle\Psi_{nk}^{(e-p)}|)$. The electronic purity of such reduced density matrix is defined as $\mathbb{P}_{nk} = \text{Tr}_{\text{el}}(\hat{\rho}_{nk}^2)$ [34] and is equal to 1 when the electron-photon eigenstate is separable and the electronic reduced density matrix is pure (not mixed). Note that decreasing purity corresponds to increasing electron-photon entanglement. For $g = 0.1$, the minimum of the electronic purity (the purity depends on \mathbf{k}) is about 75% for the top panel of Fig. 3 and 88% for the bottom one. In such configuration, one might describe the system with an effective electronic Hamiltonian [21–25]. Indeed, as shown in Fig. 2 the diagrams are qualitatively reproduced by an effective electronic Hamiltonian approach (see Supplemental Material [31]). However our electron-photon Chern number introduced in Eq. (4) and based on the exact light-matter energies $\mathcal{E}_{nk}^{(e-p)}$ is defined also for low electronic purity, i.e., for any arbitrary light-matter hybridization.

Let us now consider the situation where the cavity mode has a relatively low frequency and is resonant with electronic miniband transitions. Note that we consider here out-of-plane cavity polarization $\mathbf{u} = (0, 0, 1)$ and the corresponding dimensionless coupling constant is defined as $g_\perp = eA_0d/\hbar$. The corresponding results are depicted in Figs. 4 and 5. In the noninteracting case ($g_\perp = 0$), the photon energy creates replicas of the electronic minibands with nonzero photon numbers, as shown in Fig. 5. The bare electron-photon spectrum becomes degenerate when a photon replica crosses the original electronic miniband with zero photons. However, a finite coupling lifts such degeneracies, leading to new electron-photon energy minibands for which we can compute the electron-photon Chern number. Figure 4 shows the topological diagram

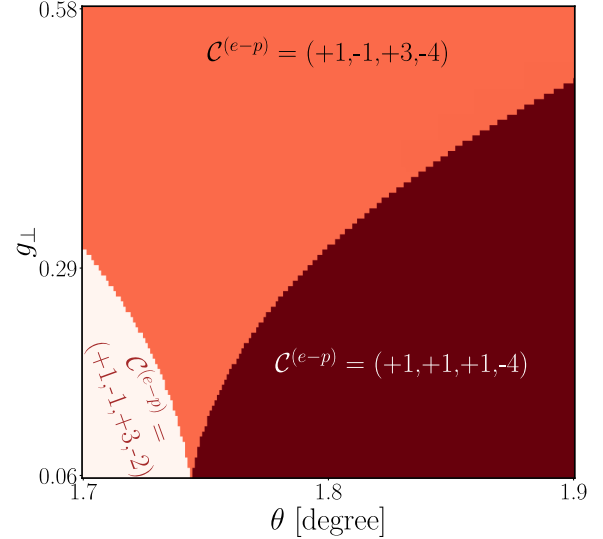


FIG. 4. Electron-photon Chern numbers of the first four moiré minibands for the considered cavity-embedded twisted TMD bilayer system. Note that this topological diagram cannot be predicted by the effective electronic model used in Fig. 2. Other parameters: cavity photon energy $\hbar\omega_c = 10$ meV, $V_z = 0$ meV, and cavity mode polarization $\mathbf{u} = (0, 0, 1)$.

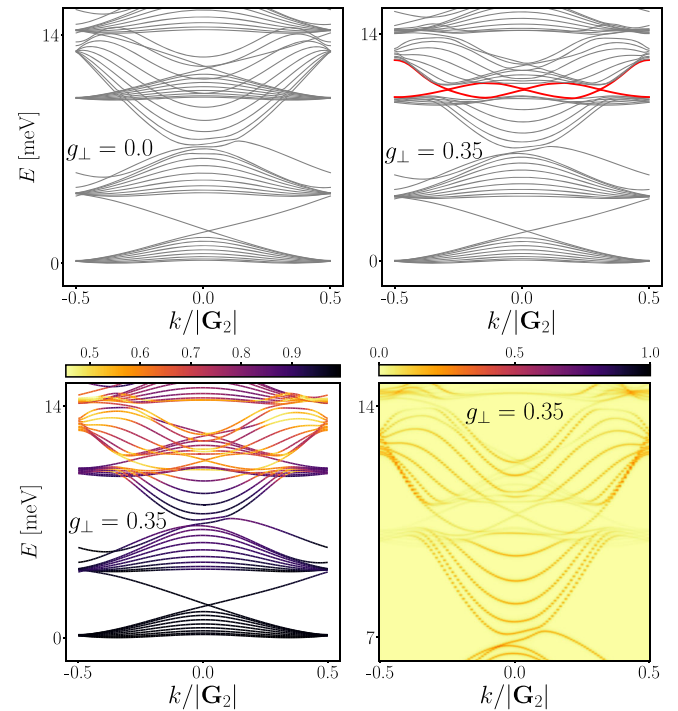


FIG. 5. Top panels: electron-photon miniband dispersions $\mathcal{E}_{nk}^{(e-p)}$ for $g_\perp = 0$ (left panel) and 0.35 (right panel), where three edge states emerge (thicker red lines). Bottom panels: electronic purity (left panel) and electronic spectral function (right panel, normalized by its maximum value) for $g_\perp = 0.35$. We have considered a ribbon geometry with width $D_1/a_M = 10$ and periodic boundary conditions along the long direction. Other parameters: cavity photon energy $\hbar\omega_c = 10$ meV, $V_z = 0$ meV, $\theta = 1.8^\circ$, cavity mode polarization $\mathbf{u} = (0, 0, 1)$.

characterized by such electron-photon Chern numbers for the first four minibands. The cavity photon energy is resonant to the transition between the first and third electronic minibands, depicted in Fig. 5. The bulk-edge correspondence for the electron-photon Chern number is satisfied: indeed, we observe three edge states shown by the thicker red line in Fig. 5. These states have low electronic purity (as low as 50%) and cannot be captured by an effective electronic Hamiltonian where the photon degrees of freedom are eliminated. Moreover, such high Chern numbers, created by the hybridization with the cavity photon replicas, are absent in the bare electronic system. These multiple new edge states corresponding to high Chern numbers, can be observed by measuring the electronic spectral function via angle-resolved photoemission spectroscopy [35], scanning tunneling microscopy [36], or microwave impedance microscopy [37].

Conclusions.—In this Letter, we explored the new topological phases characterized by the electron-photon Chern number, a topological invariant defined in terms of the exact eigenstates for the Hamiltonian describing a fermionic particle coupled to a quantized electromagnetic field. This is a topological invariant for any arbitrary hybridization of the electron-photon eigenstates. Note that electron-photon Chern numbers can also be defined for disordered and nonhomogeneous systems [38–41], so the present topological approach can also be generalized to situations where the cavity mode is not spatially homogeneous or in the presence of electronic disorder. The results of this Letter are exact when a single fermion is injected in empty minibands. A future and intriguing problem to explore is how these topological states evolve when such electron-photon states are partially filled.

We acknowledge financial support from the French agency ANR through the project NOMOS (ANR-18-CE24-0026), and TRIANGLE (ANR-20-CE47-0011), CaVdW under the ANR/RGC Joint Research Scheme sponsored by ANR and RGC of Hong Kong SAR China (ANR-21-CE30-0056-01, A-HKU705/21), and from the Israeli Council for Higher Education–VATAT. Z. L. and W. Y. also acknowledge support by RGC of Hong Kong SAR (HKU SRFS2122-7S05, AoE/P-701/20).

-
- [1] A. K. Geim and I. V. Grigorieva, van der Waals heterostructures, *Nature (London)* **499**, 419 (2013).
 - [2] P. Ajayan, P. Kim, and K. Banerjee, Two-dimensional van der Waals materials, *Phys. Today* **69**, No. 9, 38 (2016).
 - [3] K. S. Novoselov, A. Mishchenko, A. Carvalho, and A. H. C. Neto, 2D materials and van der Waals heterostructures, *Science* **353** (2016).
 - [4] J. C. W. Song and N. M. Gabor, Electron quantum metamaterials in van der Waals heterostructures, *Nat. Nanotechnol.* **13**, 986 (2018).

- [5] O. Ávalos-Ovando, D. Mastrogiuseppe, and S. E. Ulloa, Lateral heterostructures and one-dimensional interfaces in 2D transition metal dichalcogenides, *J. Phys. Condens. Matter* **31**, 213001 (2019).
- [6] M. Yankowitz, Q. Ma, P. Jarillo-Herrero, and B. J. LeRoy, van der Waals heterostructures combining graphene and hexagonal boron nitride, *Nat. Rev. Phys.* **1**, 112 (2019).
- [7] R. Bistritzer and A. H. MacDonald, Moiré bands in twisted double-layer graphene, *Proc. Natl. Acad. Sci. U.S.A.* **108**, 12233 (2011).
- [8] Y. Cao, V. Fatemi, S. Fang, K. Watanabe, T. Taniguchi, E. Kaxiras, and P. Jarillo-Herrero, Unconventional superconductivity in magic-angle graphene superlattices, *Nature (London)* **556**, 43 (2018).
- [9] K. L. Seyler, P. Rivera, H. Yu, N. P. Wilson, E. L. Ray, D. G. Mandrus, J. Yan, W. Yao, and X. Xu, Signatures of moiré-trapped valley excitons in MoSe₂/WSe₂ heterobilayers, *Nature (London)* **567**, 66 (2019).
- [10] K. Tran *et al.*, Evidence for moiré excitons in van der Waals heterostructures, *Nature (London)* **567**, 71 (2019).
- [11] C. Jin, E. C. Regan, A. Yan, M. I. B. Utama, D. Wang, S. Zhao, Y. Qin, S. Yang, Z. Zheng, S. Shi, K. Watanabe, T. Taniguchi, S. Tongay, A. Zettl, and F. Wang, Observation of moiré excitons in WSe₂/WS₂ heterostructure superlattices, *Nature (London)* **567**, 76 (2019).
- [12] P. Forn-Díaz, L. Lamata, E. Rico, J. Kono, and E. Solano, Ultrastrong coupling regimes of light-matter interaction, *Rev. Mod. Phys.* **91** (2019).
- [13] A. F. Kockum, A. Miranowicz, S. D. Liberato, S. Savasta, and F. Nori, Ultrastrong coupling between light and matter, *Nat. Rev. Phys.* **1**, 19 (2019).
- [14] F. J. Garcia-Vidal, C. Ciuti, and T. W. Ebbesen, Manipulating matter by strong coupling to vacuum fields, *Science* **373** (2021).
- [15] F. Schlawin, D. M. Kennes, and M. A. Sentef, Cavity quantum materials, *Appl. Phys. Rev.* **9**, 011312 (2022).
- [16] J. Keller, G. Scalari, S. Cibella, C. Maissen, F. Appugliese, E. Giovine, R. Leoni, M. Beck, and J. Faist, Few-electron ultrastrong light-matter coupling at 300 GHz with nanogap hybrid LC microcavities, *Nano Lett.* **17**, 7410 (2017).
- [17] G. Scalari, C. Maissen, D. Turcinkova, D. Hagenmuller, S. D. Liberato, C. Ciuti, C. Reichl, D. Schuh, W. Wegscheider, M. Beck, and J. Faist, Ultrastrong coupling of the cyclotron transition of a 2D electron gas to a THz metamaterial, *Science* **335**, 1323 (2012).
- [18] G. L. Paravicini-Bagliani, F. Appugliese, E. Richter, F. Valmorra, J. Keller, M. Beck, N. Bartolo, C. Rössler, T. Ihn, K. Ensslin, C. Ciuti, G. Scalari, and J. Faist, Magnetotransport controlled by Landau polariton states, *Nat. Phys.* **15**, 186 (2018).
- [19] F. Appugliese, J. Enkner, G. L. Paravicini-Bagliani, M. Beck, C. Reichl, W. Wegscheider, G. Scalari, C. Ciuti, and J. Faist, Breakdown of topological protection by cavity vacuum fields in the integer quantum Hall effect, *Science* **375**, 1030 (2022).
- [20] C. Ciuti, Cavity-mediated electron hopping in disordered quantum Hall systems, *Phys. Rev. B* **104** (2021).
- [21] G. Arwas and C. Ciuti, Quantum electron transport controlled by cavity vacuum fields, *Phys. Rev. B* **107** (2023).

- [22] O. Dmytruk and M. Schirò, Controlling topological phases of matter with quantum light, *Commun. Phys.* **5** (2022).
- [23] X. Wang, E. Ronca, and M. A. Sentef, Cavity quantum electrodynamical Chern insulator: Towards light-induced quantized anomalous Hall effect in graphene, *Phys. Rev. B* **99**, 235156 (2019).
- [24] J. Li, L. Schamriß, and M. Eckstein, Effective theory of lattice electrons strongly coupled to quantum electromagnetic fields, *Phys. Rev. B* **105** (2022).
- [25] D. Guerci, P. Simon, and C. Mora, Superradiant phase transition in electronic systems and emergent topological phases, *Phys. Rev. Lett.* **125**, 257604 (2020).
- [26] K. Masuki and Y. Ashida, Berry phase and topology in ultrastrongly coupled quantum light-matter systems, *Phys. Rev. B* **107** (2023).
- [27] T. Karzig, C.-E. Bardyn, N. H. Lindner, and G. Refael, Topological polaritons, *Phys. Rev. X* **5**, 031001 (2015).
- [28] T. Ozawa, H. M. Price, A. Amo, N. Goldman, M. Hafezi, L. Lu, M. C. Rechtsman, D. Schuster, J. Simon, O. Zilberberg, and I. Carusotto, Topological photonics, *Rev. Mod. Phys.* **91**, 015006 (2019).
- [29] F. Wu, T. Lovorn, E. Tutuc, I. Martin, and A. MacDonald, Topological insulators in twisted transition metal dichalcogenide homobilayers, *Phys. Rev. Lett.* **122** (2019).
- [30] D. Zhai and W. Yao, Theory of tunable flux lattices in the homobilayer Moiré of twisted and uniformly strained transition metal dichalcogenides, *Phys. Rev. Mater.* **4** (2020).
- [31] See Supplemental Material at <http://link.aps.org/supplemental/10.1103/PhysRevLett.131.176602> for additional details about the cavity QED Hamiltonian, the purity of electronic reduced density matrix, the spectral functions, and spatial distribution of edge states.
- [32] H. Yu, M. Chen, and W. Yao, Giant magnetic field from Moiré induced Berry phase in homobilayer semiconductors, *Natl. Sci. Rev.* **7**, 12 (2020).
- [33] R. Zhao, G.-D. Xie, M. L. N. Chen, Z. Lan, Z. Huang, and W. E. I. Sha, First-principle calculation of Chern number in gyrotropic photonic crystals, *Opt. Express* **28**, 4638 (2020).
- [34] C. Cohen-Tannoudji, B. Diu, and F. Laloë, *Mécanique Quantique: Tome 1* (EDP Sciences, Les Ulis, France, 2020).
- [35] R. Noguchi *et al.*, Evidence for a higher-order topological insulator in a three-dimensional material built from van der Waals stacking of bismuth-halide chains, *Nat. Mater.* **20**, 473 (2021).
- [36] C. Tao, L. Jiao, O. V. Yazyev, Y.-C. Chen, J. Feng, X. Zhang, R. B. Capaz, J. M. Tour, A. Zettl, S. G. Louie, H. Dai, and M. F. Crommie, Spatially resolving edge states of chiral graphene nanoribbons, *Nat. Phys.* **7**, 616 (2011).
- [37] M. E. Barber, E. Y. Ma, and Z.-X. Shen, Microwave impedance microscopy and its application to quantum materials, *Nat. Rev. Phys.* **4**, 61 (2021).
- [38] E. Prodan, T. L. Hughes, and B. A. Bernevig, Entanglement spectrum of a disordered topological Chern insulator, *Phys. Rev. Lett.* **105** (2010).
- [39] R. Bianco and R. Resta, Mapping topological order in coordinate space, *Phys. Rev. B* **84**, 241106(R) (2011).
- [40] Y.-F. Zhang, Y.-Y. Yang, Y. Ju, L. Sheng, R. Shen, D.-N. Sheng, and D.-Y. Xing, Coupling-matrix approach to the Chern number calculation in disordered systems, *Chin. Phys. B* **22**, 117312 (2013).
- [41] M. D. Caio, G. Möller, N. R. Cooper, and M. J. Bhaseen, Topological marker currents in Chern insulators, *Nat. Phys.* **15**, 257 (2019).